Evidence of quantum dimer excitations in $Sr_3Ir_2O_7$

M. Moretti Sala,[1,*] V. Schnells,[2,*] S. Boseggia,[3,4] L. Simonelli,[1,5] A. Al-Zein,[1] J. G. Vale,[3] L. Paolasini,[1] E. C. Hunter,[6] R. S. Perry,[3] D. Prabhakaran,[7] A. T. Boothroyd,[7] M. Krisch,[1] G. Monaco,[1,8] H. M. Rønnow,[9,10] D. F. McMorrow,[3] and F. Mila[11]

[1] *European Synchrotron Radiation Facility, BP 220, F-38043 Grenoble Cedex, France*
[2] *Institute for Theoretical Physics and Astrophysics, University of Würzburg, Am Hubland D-97074 Würzburg, Germany*
[3] *London Centre for Nanotechnology and Department of Physics and Astronomy, University College London, London WC1E 6BT, UK*
[4] *Diamond Light Source Ltd, Diamond House, Harwell Science and Innovation Campus, Didcot, Oxfordshire OX11 0DE, UK*
[5] *CELLS-ALBA Synchrotron Radiation Facility, Carretera BP 1413, km 3.3 08290 Cerdanyola del Valles, Barcelona, Spain*
[6] *Centre for Science at Extreme Conditions, Peter Guthrie Tait Road, King's Buildings, Edinburgh. EH9 3FD. United Kingdom*
[7] *Clarendon Laboratory, Department of Physics, University of Oxford, Parks Road, Oxford, OX1 3PU, United Kingdom*
[8] *Dipartimento di Fisica, Università di Trento, via Sommarive 14, 38123 Povo (TN), Italy*
[9] *Laboratory for Quantum Magnetism, École Polytechnique Fédérale de Lausanne (EPFL), CH-1015 Lausanne, Switzerland*
[10] *Neutron Science Laboratory, Institute for Solid State Physics, University of Tokyo, Kashiwa, Chiba 277-8581, Japan*
[11] *Institute of Theoretical Physics, École Polytechnique Fédérale de Lausanne (EPFL), CH-1015 Lausanne, Switzerland*

(Dated: June 17, 2015)

The magnetic excitation spectrum in the bilayer iridate $Sr_3Ir_2O_7$ has been investigated using high-resolution resonant inelastic x-ray scattering (RIXS) performed at the iridium L_3 edge and theoretical techniques. A study of the systematic dependence of the RIXS spectrum on the orientation of the wavevector transfer, **Q**, with respect to the iridium-oxide bilayer has revealed that the magnon dispersion is comprised of two branches well separated in energy and gapped across the entire Brillouin zone. Our results contrast with those of an earlier study which reported the existence of a single dominant branch. While these earlier results were interpreted as two overlapping modes within a spin-wave model of weakly coupled iridium-oxide planes, our results are more reminiscent of those expected for a system of weakly coupled dimers. In this latter approach the lower and higher energy modes find a natural explanation as those corresponding to transverse and longitudinal fluctuations, respectively. We have therefore developed a bond-operator theory which describes the magnetic dispersion in $Sr_3Ir_2O_7$ in terms of quantum dimer excitations. In our model dimerisation is produced by the leading Heisenberg exchange, J_c, which couples iridium ions in adjacent planes of the bilayer. The Hamiltonian also includes in plane exchange, J, as well as further neighbour couplings and relevant anisotropies. The bond-operator theory provides an excellent account of the dispersion of both modes, while the measured **Q** dependence of the RIXS intensities is in reasonable qualitative accord with the spin-spin correlation function calculated from the theory. We discuss our results in the context of the quantum criticality of bilayer dimer systems in the presence of anisotropic interactions derived from strong spin-orbit coupling.

I. INTRODUCTION

The physics of iridium-based $5d$ transition-metal oxides has triggered considerable interest, as it represents the opportunity to explore the consequences of electron correlations in the strong spin-orbit coupling limit. Various novel electronic states, topological and otherwise, have been predicted for the iridates[1,2]. The most studied example to date is the relativistic Mott-like insulating state observed in Sr_2IrO_4 which, in the absence of spin-orbit coupling, would be expected to be a metal. The insulating state has been argued to result from the combined action of strong crystal-field and spin-orbit coupling, leading to band narrowing and a $j_{\rm eff} = 1/2$ ground state, on which electron correlations then act to produce a charge energy gap ΔE[3].

More generally, studies of the Ruddlesden-Popper series, $Sr_{n+1}Ir_nO_{3n+1}$, are proving to be particularly fruitful, as members of this series display a striking evolution in their electronic and magnetic properties as the number of IrO_2-layers is increased. This can be illustrated by considering the end members of this series. Single layer $Sr_2IrO_4 (n = 1)$ is an insulator ($\Delta E \approx 615$ meV[5]) with a canted, basal-plane antiferromagnetic (AF) ground state[6,7], displaying a magnon dispersion[8] consistent with an effective Hamiltonian dominated by Heisenberg interactions, in agreement with theory[9]. $SrIrO_3$ $(n = \infty)$ is a strongly correlated metal with ferromagnetic correlations[10]. Bilayer $Sr_3Ir_2O_7$ $(n = 2)$ represents the

* Both authors contributed equally.

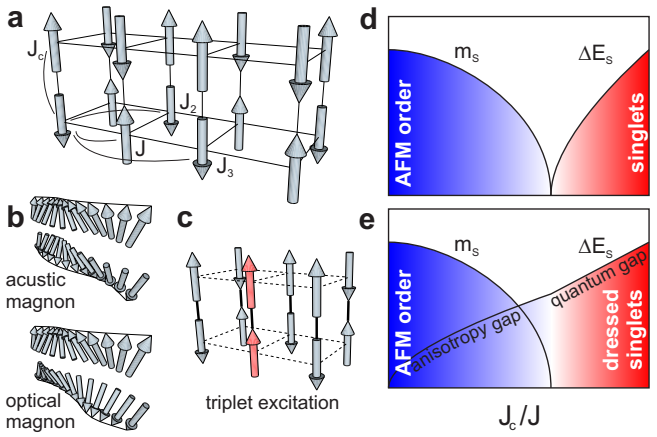

FIG. 1. (a)-(c) Magnetic structure and excitations in $Sr_3Ir_2O_7$. (a) intra and inter-layer couplings (see Eq. 1); (b) conventional acoustic and optical spin-wave modes previously used to interpret RIXS data from $Sr_3Ir_2O_7$[4]; (c) dimer triplet excitation. (d)-(e) Schematic evolution of a bilayer system as a function of inter- to intra-layer coupling. (d) Quantum phase transition of the SU(2) symmetric model; (e) Effect of anisotropy leading to a cross over between antiferromagnetic order and quantum dimer regime with a gap ΔE_S that never closes for finite coupling ratios.

interesting case of being a marginal insulator ($\Delta E \approx 130$ meV[11]), with a c-axis antiferromagnetic ground state (Fig. 1(a))[12,13], and a magnetic spectrum dominated by a single excitation with an unusually large magnon energy gap $\Delta E_S \sim 85$ meV[4].

This excitation has been interpreted as two overlapping bilayer spin-wave modes (Fig. 1(b)) in the presence of enhanced interlayer pseudo-dipolar coupling[4]. However, in bilayer systems, the presence of a single dominant magnon branch is typical of weakly coupled dimers, in which case anisotropy generically gives rise to two gapped modes close to each other with significantly different intensities. Therefore, we reexamine the nature of the low-energy dynamics in $Sr_3Ir_2O_7$ by performing high-resolution resonant inelastic X-ray scattering (RIXS) experiments which exploit a different experimental geometry compared to Ref. 4. Our experiment establishes a fundamentally different picture of the magnon dispersion in $Sr_3Ir_2O_7$, with the observation of two distinct gapped modes. The dispersion and intensity of these modes are hard to reconcile with a spin-wave description, but they can be well accounted for by a bond-operator mean-field description that captures the quantum dimer nature of the excitations (Fig. 1(c)).

II. EXPERIMENTAL

RIXS is a photon in–photon out technique for the investigation of the electronic structure of materials by probing excitations of various nature[14]. The scattering process can be described as in the following: a monochromatic photon is resonantly absorbed by the system, promoting an electron from a core level into the valence band. This state, usually referred to as the intermediate state of the RIXS process, is highly unstable and therefore short-lived. In RIXS one monitors the recombination of the core-hole to a final state of lower energy by a radiative transition. Analysis of the energy and momentum of the emitted photon allows one to characterise the final state of the RIXS process; this can be either the ground state itself, as in elastic scattering, in which case the emitted photon energy coincides with the inident one, or an excited state. In the latter case, the energy of the excited state is determined by the difference between the incident and emitted photon energy. Beside energy, momentum transfer is also used to label excitations. This is particularly informative when studying dispersive excitations, like magnetic one.

RIXS experiments were performed on the ID20 beamline of the European Synchrotron Radiation Facility (ESRF), Grenoble, with an overall energy resolution of 25 meV. This is achieved by monochromatising the incident photons with a Si(844) back-scattering channel-cut and using a Rowland spectrometer equipped with Si(844) spherical (R=2 m) diced crystal analysers[15]. The scattering plane and incident photon polarisation were both horizontal in the laboratory frame, i.e. π incident polarization was used. The $Sr_3Ir_2O_7$ single crystal was grown by flux method of Ref. 12. The sample was cooled to a temperature of 15 K in a closed flow He-cryostat equipped with Be-windows. RIXS spectra were recorded with the incident photon energy fixed at 11.217 keV, approximately 3 eV below the main absorption line as it is known that the intensity of magnetic excitations is maximized at this energy[16–18]. This shift provides a rough estimate of the cubic crystal-field splitting in Ir $5d$ states consistent with previous results[19].

In Fig. 2(a), we present the in-plane momentum dependence of the RIXS response from $Sr_3Ir_2O_7$ along high-symmetry directions of the Brillouin zone for $L = 28.5$. An elastic line (possibly containing contributions from phonons) and a magnetic excitation dominate the spectra in the 0−300 meV energy range. Following the convention in Ref. 4, we label these features A and B, respectively. The latter has a sizeable dispersion of 85 ± 5 meV, and a gap of comparable magnitude. A weaker feature, C, follows the dispersion of feature B at higher energies. These observations are in good accord with previous RIXS measurements[4]. However, closer inspection of the dispersion along the symmetry line from (0,0) to (1/4,1/4), reveals the presence of an additional, previously unreported feature, labelled D. This is most prominent around (0,0) where it is clearly separated from B and C. Away from (0,0), it merges almost into feature B and contributes to its lineshape and spectral weight. The intensity of feature D was found to be strongly dependent on the out-of-plane component of $\mathbf{Q}$: it completely vanishes when changing L from 28.5 to 25, as shown in the two panels of Fig. 2(b).

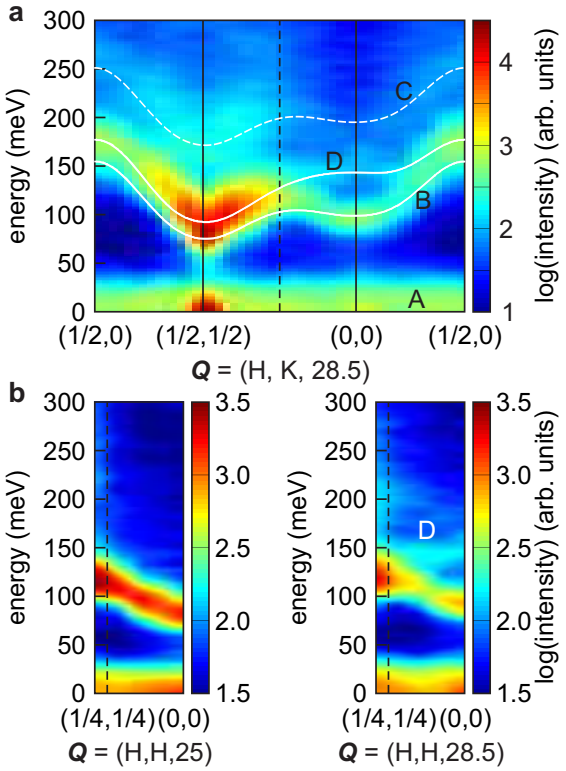

FIG. 2. In-plane wavevector dependence of the RIXS response of $Sr_3Ir_2O_7$ in the 0-300 meV energy range. (a) High-symmetry directions, $\mathbf{Q} = (H, K, 28.5)$ (r.l.u.). Letters A-D label modes discussed in the text. White lines represent our model. (b) Close-up on limited region of the Brillouin zone, $\mathbf{Q} = (H, H, 25)$ (left) and $\mathbf{Q} = (H, H, 28.5)$ (right).

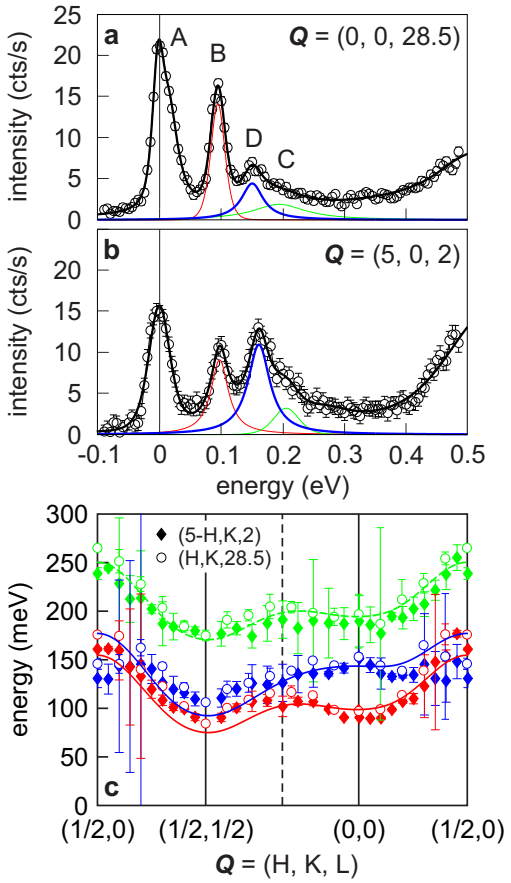

FIG. 3. (a)-(b) RIXS spectra from $Sr_3Ir_2O_7$ for (a) $\mathbf{Q} = (0, 0, 28.5)$ and (b) $\mathbf{Q} = (5, 0, 2)$. (c) Energies of features B (red), C (green) and D (blue) as a function of in-plane momentum transfer. Experimental data: open circles, (H, K, 28.5), filled diamonds, (5-H,K,2). Theory: continuous lines represent the transverse (red) and longitudinal (blue) modes, respectively. As in Fig. 2(a), the dashed line is a guide to the eye obtained by shifting the theoretical curve for feature B by approximately 85 meV.

The spectrum corresponding to $\mathbf{Q} = (0, 0, 28.5)$ is displayed in Fig. 3(a). Features B, C and D are fitted to three Pearson VII functions[20]. Feature D is clearly visible, although its integrated intensity is only a fraction of that of B and comparable to that of C. The extracted dispersions of features B, C and D as a function of the in-plane momentum transfer for $L = 28.5$ are plotted in Fig. 3(c). The corresponding wavevector dependences of the integrated intensities are shown in Fig. 4(a).

The results discussed so far were obtained in a geometry with the wavevector transfer $\mathbf{Q}$ predominantly perpendicular to the IrO_2 planes. To explore how the RIXS spectrum depends on the orientation of $\mathbf{Q}$, experiments were also performed with $\mathbf{Q}$ predominatly oriented in the IrO_2 planes. An example of data taken in this geometry is shown in Fig. 3(b). It is immediately clear that the relative peak intensities of the features have a strong dependence on the orientation of $\mathbf{Q}$, with feature D acquiring spectral weight at the expense of feature B as $\mathbf{Q}$ is rotated towards the planes. The energies and intensities extracted from data taken with $\mathbf{Q}$ in-plane are also plotted in Fig. 3(c) and Fig. 4(a), respectively, where they are seen to be in good agreement with data acquired using the initial geometry.

Features B and C have already been identified and discussed in Ref. 4. Feature B was interpreted as the superposition of almost degenerate acoustic and optical magnons (Fig. 1(b)), and their dispersion was modelled on the basis of a Hamiltonian which includes intra- and interlayer couplings, as well as pseudo-dipolar and Dzyaloshinsky-Moriya interaction terms. Feature C was assigned to the onset of a multi-magnon continuum. Feature D was not reported in the previous experiment, most likely because of the nontrivial dependence of its intensity on momentum transfer both as a function of L (Fig. 2(b)) and the orientation of $\mathbf{Q}$ (Fig. 3(a) and (b)) revealed here.

III. THEORY

Let us now turn to a theoretical discussion of the magnetic excitations of $Sr_3Ir_2O_7$. In a SU(2) symmetric (Heisenberg) bilayer system, there is a quantum phase transition as a function of the ratio of interlayer to intralayer coupling[21–27] between a gapless, magnetically ordered phase, and a gapped phase (see Fig.1(d)). In the limits of very weak or very strong inter-layer coupling, linear spin-wave theory and perturbation theory starting from isolated dimers provide very accurate descriptions respectively. However, these approaches fail in the intermediate regime, and the only simple approach that provides a qualitatively correct description throughout is the bond-operator mean-field theory[26,28–31].

In the presence of strong anisotropy, as is the case in $Sr_3Ir_2O_7$, the excitation spectrum is always gapped (Fig. 1(e)), and it is impossible to know just from the excitation spectrum in which regime the system lies. However, on general grounds the excitation spectrum of $Sr_3Ir_2O_7$ revealed by RIXS is incompatible with linear spin-wave theory. Indeed linear spin-wave theory predicts two modes, which have dispersions related to each other by $\omega_{\rm acustic}(\mathbf{q}) = \omega_{\rm optical}((1/2,1/2)-\mathbf{q})$ ($\mathbf{q}$ is the in-plane momentum transfer), implying that the spectrum should be symmetric around $(1/4,1/4)$ in Fig. 3(c), which is clearly not the case.

We therefore developed a description of $Sr_3Ir_2O_7$ in terms of coupled dimers. In this approach, the parameter that controls the center of the main band is the interlayer coupling J_c, which must then be of the order of 100 meV. The fact that the dispersion is approximately degenerate at (1/2,1/2) points to a dominant intra-plane ferromagnetic diagonal inter-dimer coupling. Finally, Hund's rule exchange and the staggered rotation of the Ir-O octahedra are known to induce anisotropic pseudo-dipolar and Dzyaloshinskii-Moriya interactions[32]. We therefore consider the Hamiltonian

$$\begin{aligned} H =& J \sum_{<i,j>,l} \Big[\cos(2\theta)\mathbf{S}_{li}\cdot\mathbf{S}_{lj} + 2\sin^2(\theta) S^z_{li} S^z_{lj} + \\ & - \epsilon_i\epsilon_l \sin(2\theta)(\mathbf{S}_{li}\times\mathbf{S}_{lj})\cdot\hat{e}_z \Big] + J_c \sum_i \mathbf{S}_{1i}\cdot\mathbf{S}_{2i} \\ & + J_2 \sum_{\ll i,j\gg,l} \mathbf{S}_{li}\cdot\mathbf{S}_{lj} + J_3 \sum_{\lll i,j\ggg,l} \mathbf{S}_{li}\cdot\mathbf{S}_{lj}, \qquad (1) \end{aligned}$$

where, in agreement with Sr_2IrO_4, a third neighbor in-plane coupling has been included[8]. The naming convention for the exchange constants is indicated in Fig. 1(a). In principle, due to the staggered rotation of IrO_6 octahedra, all bonds connecting opposite sublattices have anisotropic exchange contributions, but one can gauge away some of them[33], e.g. that on the interlayer coupling J_c, which we have chosen to do. In single layer Sr_2IrO_4 the angle θ can be inferred directly from the canting of the in-plane ordered moment[34]. In $Sr_3Ir_2O_7$ the moments order along the c-axis, and θ is a just a measure of the relative strength of the anisotropic interactions.

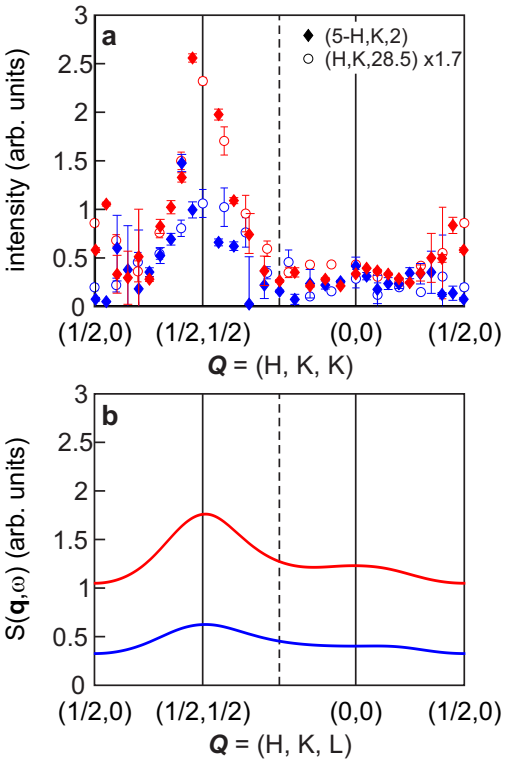

FIG. 4. Integrated intensity of features B and D as a function of in-plane momentum transfer. (a) Experimental data for features B (red) and D (blue): open circles, (H, K, 28.5), filled diamonds, (5-H,K,2). (b) Theory: transverse (red) and longitudinal (blue) responses.

A. Bond-operator mean-field method

This model has been treated using bond-operator mean-field theory introduced by Sachdev and Bhatt[28], which has proved to be an accurate method for many bilayer spin systems and was especially applied to spin ladder systems[29–31]. In this formalism, first of all, a close-packed dimerization of the lattice is chosen. In the case of our bilayer system, we designate interlayer bonds on the sites $(1,i)-(2,i)$, where the first coordinate refers to the layer and the second one to the position inside the layer. The four states $|\uparrow\downarrow\rangle$, $|\downarrow\uparrow\rangle$, $|\uparrow\uparrow\rangle$ and $|\downarrow\downarrow\rangle$ on each rung i in the Hilbert space can be combined to form one singlet state $|s_i\rangle$ and three triplet states $|t^\alpha_i\rangle$, α=x,y,z. To do so, singlet and triplet creation operators that create the

states out of the vacuum $|0\rangle$ are introduced

$$\begin{aligned}
|s_i\rangle \equiv& s_i^\dagger |0\rangle = \frac{1}{\sqrt{2}}(|\uparrow\downarrow\rangle - |\downarrow\uparrow\rangle),\\
|t_i^x\rangle \equiv& t_i^{x,\dagger} |0\rangle = -\frac{1}{\sqrt{2}}(|\uparrow\uparrow\rangle - |\downarrow\downarrow\rangle),\\
|t_i^y\rangle \equiv& t_i^{y,\dagger} |0\rangle = \frac{\mathrm{i}}{\sqrt{2}}(|\uparrow\uparrow\rangle + |\downarrow\downarrow\rangle),\\
|t_i^z\rangle \equiv& t_i^{z,\dagger} |0\rangle = \frac{1}{\sqrt{2}}(|\uparrow\downarrow\rangle + |\downarrow\uparrow\rangle).
\end{aligned} \tag{2}$$

On each rung, the operators must fulfill a local hard-core constraint $s_i^\dagger s_i + \sum_\alpha t_i^{\alpha,\dagger} t_i^\alpha = 1,\ \alpha = x, y, z$. The action of the spin operators on the singlet and triplet states is then equivalent to

$$\begin{aligned}
\mathbf{S}_{1,i}^\alpha &= \frac{1}{2}\left(s_i^\dagger t_i^\alpha + t_i^{\alpha,\dagger} s_i - \mathrm{i}\sum_{\beta,\gamma} \epsilon_{\alpha\beta\gamma} t_i^{\beta,\dagger} t_i^\gamma \right),\\
\mathbf{S}_{2,i}^\alpha &= \frac{1}{2}\left(-s_i^\dagger t_i^\alpha - t_i^{\alpha,\dagger} s_i - \mathrm{i}\sum_{\beta,\gamma} \epsilon_{\alpha\beta\gamma} t_i^{\beta,\dagger} t_i^\gamma \right).
\end{aligned} \tag{3}$$

1. *Dispersion*

To implement the mean-field approximation, one has to make assumptions about the ground state. Experimentally, it is known that the system has easy c-axis collinear AF magnetic order. We therefore describe the ground state by a condensation of singlet and triplet t^z operators, $|GS\rangle = \prod_i \tilde{s}_i^\dagger$, $\langle \tilde{s} \rangle \neq 0$, where a new operator basis is defined through rotation with a rotation angle χ adjusted to eliminate linear terms in the bosonic Hamiltonian, $4\,(J - J_2 - J_3)\cos(2\chi) = J_c$:

$$\begin{aligned}
\tilde{s}_i^\dagger =& \cos(\chi) s_i^\dagger - \epsilon_i \sin(\chi) t_i^{z,\dagger},\ \tilde{t}_i^{x,\dagger} = t_i^{x,\dagger},\\
\tilde{t}_i^{y,\dagger} =& t_i^{y,\dagger},\ \tilde{t}_i^{z,\dagger} = \epsilon_i \sin(\chi) s_i^\dagger + \cos(\chi) t_i^{z,\dagger}.
\end{aligned} \tag{4}$$

Here, $\epsilon_i = e^{i\mathbf{Q}\cdot\mathbf{R}_i}$ with $\mathbf{q} = (\pi, \pi)$. Inserting this representation into the Hamiltonian of Eq.(1), some simplifications are possible: three-triplet terms have no contribution since they change sign under reflection along a plane perpendicular to the c-axis and passing through the centre of the rungs. Therefore, they vanish when taking the expectation value[29]. Additionally, quartic triplet terms can be neglected due to their marginal effect on the results. This corresponds to ignoring triplet-triplet interactions.

The resulting Hamiltonian can be easily diagonalized with the help of a Bogoliubov transformation. We obtain a longitudinal mode $\omega_{\mathbf{q},z}$ and a two-fold degenerate transverse mode $\omega_{\mathbf{q},x} = \omega_{\mathbf{q},y}$

$$\omega_{\mathbf{q},\alpha} = \sqrt{A_{\mathbf{q},\alpha}^2 - |B_{\mathbf{q},\alpha}|^2}, \tag{5}$$

with $\alpha = x, y, z$ and

$$\begin{aligned}
A_{\mathbf{q},z} =& 4J\left[\sin^2(2\chi)\left(1 - \frac{J_2}{J} - \frac{J_3}{J}\right) + \frac{J_c}{4J}\cos(2\chi)\right] + \frac{J}{2}\left[\cos^2(2\chi)\gamma_\mathbf{q} + \frac{J_2}{J}\delta_\mathbf{q} + \frac{J_3}{J}\varphi_\mathbf{q}\right],\\
B_{\mathbf{q},z} =& \frac{J}{2}\left[\cos^2(2\chi)\gamma_\mathbf{q} + \frac{J_2}{J}\delta_\mathbf{q} + \frac{J_3}{J}\varphi_\mathbf{q}\right],\\
A_{\mathbf{q},\tau} =& 2J\left[\frac{J_c}{2J}\cos^2(\chi) + \sin^2(2\chi)\left(1 - \frac{J_2}{J} - \frac{J_3}{J}\right)\right] + \frac{J}{2}\left[\cos(2\theta)\cos(2\chi)\right]\gamma_\mathbf{q} + \frac{J_2}{2}\delta_\mathbf{q} + \frac{J_3}{2}\varphi_\mathbf{q},\\
B_{\mathbf{q},\tau} =& \frac{J}{2}\left[\cos(2\theta) - \mathrm{i}\sin(2\theta)\sin(2\chi)\right]\gamma_\mathbf{q} + \frac{J_2}{2}\cos(2\chi)\delta_\mathbf{q} + \frac{J_3}{2}\cos(2\chi)\varphi_\mathbf{q},
\end{aligned} \tag{6}$$

where $\delta_\mathbf{q} = 2(\cos(q_x + q_y) + \cos(q_x - q_y))$, $\gamma_\mathbf{q} = 2(\cos q_x + \cos q_y)$, $\varphi_\mathbf{q} = 2(\cos 2q_x + \cos 2q_y)$, and $\tau = x, y$.

As long as $\chi > 0$, the gap of the transverse mode at $\mathbf{q} = (\pi, \pi)$ is given by

$$\Delta E_S = \sqrt{J J_c}\sqrt{\frac{4J_2 + 4J_3 - 4J - J_c}{J_2 + J_3 - J}}\sin(2\theta). \tag{7}$$

In the absence of anisotropy ($\theta = 0$), the model has two phases: i) An ordered phase with a finite staggered moment as long as $\chi > 0$. There is a Goldstone mode at (π, π), and this phase is thus gapless (the gap of Eq.(7) vanishes for $\theta = 0$); ii) A gapped, disordered phase with no staggered magnetization when $\chi = 0$. The gap closes at the transition. This is illustrated in Fig. 5(a). In the presence of anisotropy ($\theta \neq 0$), as in the bilayer iridate system, there is still a phase transition at which the staggered magnetization disappears, but the transverse mode acquires a gap in the ordered phase, as emphasized in Eq.(7). Accordingly, in the disordered phase, the gap does not vanish at the transition. This is illustrated in Fig. 5(b). In view of its properties, a reduced but still significant staggered magnetization and a large gap, we think that the compound $Sr_3Ir_2O_7$ lies in the intermediate range, on the left of the transition.

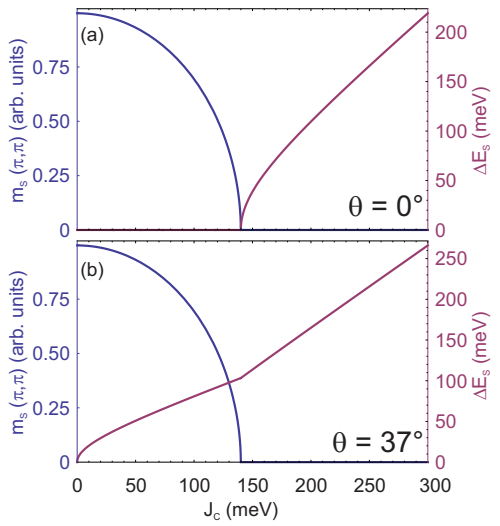

FIG. 5. Staggered magnetization m_S and magnetic gap Δ_S as a function of the interlayer coupling J_c for (a) the isotropic case ($\theta = 0°$) and (b) the anisotropic case ($\theta = 37°$). The other coupling constants are equal to $J = 26$ meV, $J_2 = -15$ meV and $J_3 = 6$ meV. In both cases, the rotation angle χ vanishes for $J_c \geq 140$ meV, bringing the system into the disordered phase.

2. Intensity

The dynamical scattering function $I^{\beta}_{q_c}(\mathbf{q},\omega)$, $\beta = x, y, z$ is proportional to the spin-spin correlation function $S^{\beta\beta}_{q_c}(\mathbf{q},\omega)$ given by

$$S^{\beta\beta}_{q_c}(\mathbf{q},\omega) = \frac{2\pi}{L}\sum_{\lambda} |\langle\lambda| S^{\beta}_{q_c}(\mathbf{q}) |0\rangle|^2 \delta(\omega + \omega_0 - \omega_\lambda) \quad (8)$$

at zero temperature with the symmetric ($q_c = 0$) and antisymmetric ($q_c = \pi$) rung operators defined in real space as $S^{\beta}_{j,q_c} := S^{\beta}_{1,j} \pm S^{\beta}_{2,j}$. The excited states $|\lambda\rangle$ are the lowest excited states with only one triplet excitation and an energy ω_λ. The energy of the ground state $|0\rangle$ is ω_0. Here, $\mathbf{q}$ is a two-dimensional vector describing the in-plane momentum transfer and q_c is the phase of the out-of-plane momentum of the excitations. Note that the relation between q_c and the out-of-plane momentum L measured in experiment is given by $q_c = 2\pi L d/c (\mathrm{mod}.2\pi)$, where $c = 20.8$ $\mathring{A}$ denotes the lattice parameter perpendicular to the bilayer, and $d = 5.1$ $\mathring{A}$ is the intralayer distance.

Evaluating Eq.(8) using the bond-operator method, we obtain expressions for the symmetric and antisymmetric part of the transverse ($I^T_{q_c}$) and longitudinal ($I^L_{q_c}$) intensities. Since the transverse dispersion branch is twofold degenerate, its intensity is the sum of the intensities of the two degenerate modes $I^T_{q_c} = I^x_{q_c} + I^y_{q_c}$. This leads to the integrated intensities

$$\begin{aligned} I^T_0(\mathbf{q}) &\propto 2\sin^2(\chi)\frac{A_{-\mathbf{q}+\pi,\tau} + \mathrm{Re}(B_{-\mathbf{q}+\pi,\tau})}{\omega_{-\mathbf{q}+\pi,\tau}}, \\ I^T_\pi(\mathbf{q}) &\propto 2\cos^2(\chi)\frac{A_{\mathbf{q},\tau} - \mathrm{Re}(B_{\mathbf{q},\tau})}{\omega_{\mathbf{q},\tau}}, \\ I^L_0(\mathbf{q}) &= 0, \\ I^L_\pi(\mathbf{q}) &\propto \cos^2(2\chi)\frac{A_{\mathbf{q},z} - \mathrm{Re}(B_{\mathbf{q},z})}{\omega_{\mathbf{q},z}}. \end{aligned} \quad (9)$$

Remarkably, the longitudinal intensity has no symmetric part.

For a three-dimensional stacking of bilayers, the dynamical scattering function is a linear combination of the symmetric and antisymmetric ones, with coefficients which depend on the out-of-plane momentum according to:

$$\begin{aligned} &I^{T/L}(\mathbf{q}, q_c, \omega) \\ &\quad\propto \cos(\frac{q_c}{2})^2 I^{T/L}_0(\mathbf{q},\omega) + \sin(\frac{q_c}{2})^2 I^{T/L}_\pi(\mathbf{q},\omega). \end{aligned} \quad (10)$$

3. Staggered magnetization

Finally, the antiferromagnetic structure of $Sr_3Ir_2O_7$ can be theoretically reproduced by calculating the staggered magnetization $m_S(\mathbf{q})$ with $\mathbf{q} = (\pi, \pi)$. Since bond-operator theory breaks rotational symmetry in the antiferromagnetically ordered phase, the staggered magnetization can be obtained via the ground state expectation value at zero temperature of the local spin operator projected along the c-axis

$$m_S(\mathbf{q}) = g\mu_B \left|\langle 0| S^z_l(\mathbf{q}) |0\rangle\right| \quad (11)$$

where $l = 1$ or 2 refers to the layer, μ_B is the Bohr magneton and $g = 2$ the electron spin g-factor. Expressing Eq.(11) via bond-operator method, we obtain

$$m_S(\mathbf{q}) = \frac{g\mu_B}{2}\left|1 - \alpha\right| \left|\sin(2\chi)\right| \quad (12)$$

where $\alpha = \frac{1}{\pi^2}\int_0^\pi d\mathrm{k}_x \int_0^\pi d\mathrm{k}_y |v^z_{\mathbf{k}}|^2$ keeps track of the reduction of the staggered magnetization due to quantum fluctuations. In this expression, $v^z_{\mathbf{k}}$ is one of the coefficients of the Bogoliubov transformation $u^z_{\mathbf{q}}$ and $v^z_{\mathbf{q}}$, which can be expressed in terms of the dispersion given in Eq.(5) as

$$u^z_{\mathbf{q}} = \sqrt{\frac{A_{\mathbf{q},z} + \omega_{\mathbf{q},z}}{2\omega_{\mathbf{q},z}}}, \quad v^z_{\mathbf{q}} = \frac{B_{\mathbf{q},z}}{\sqrt{2\omega_{\mathbf{q},z}(A_{\mathbf{q},z} + \omega_{\mathbf{q},z})}}. \quad (13)$$

B. Discussion

The results of the bond-operator mean-field theory applied to a bilayer with significant interlayer coupling and

some anisotropy can be summarized as follows: i) there is a main band of transverse excitations whose dispersion reflects to a large extent the Fourier transform of the inter-dimer coupling; ii) the anisotropic couplings induce a longitudinal excitation with a well-defined dispersion whose energy is comparable to that of the main excitation band (by contrast in the SU(2)-symmetric case longitudinal excitations only consist of a continuum of two-magnon excitations); iii) the intensity of the transverse excitation is larger than that of the longitudinal one, and it peaks at (1/2,1/2), with a ratio to the smallest intensity typically in the range 1.5-3.

Remarkably, all of the characteristics of our model are qualitatively consistent with the experimental results. Features B and D are ascribed to transverse and longitudinal excitations, respectively. Feature C is the lower boundary of the two-magnon continuum, which will be dominated by the dispersion of B shifted up in energy by the 85 meV gap, as indicated by the dashed lines in Figs. 2(a) and 3(c). In other words, regardless of the details of the model, the assumption that the system can be described as coupled dimers with some anisotropy leads to predictions that are supported by our new RIXS data. To go beyond this qualitative observation, and in the absence of strong constraints provided by e.g. *ab initio* calculations, we optimized the parameter set that agrees best with the dispersion of both modes and their intensity: $J = 26$ meV, $J_2 = -15$ meV, $J_3 = 6$ meV, $J_c = 90$ meV, and $\theta = 37°$. The dispersion curves calculated for this parameter set are plotted in Fig. 2(a) and Fig. 3(c).

The only aspect of the dispersion that is not accurately reproduced by our theory is the fact that the longitudinal mode seems to lie below the transverse one at $(\pi, 0)$. We note however that, according to a very recent improvement of the bond-order mean-field theory in the context of a $1/d$ expansion[35,36], the main effect of quantum fluctuations for a simple bilayer model in $d = 2$ is to modify the spectrum of the longitudinal mode except at $(0, 0)$, while leaving the transverse mode unaffected. So this discrepancy is likely an artefact of the bond-order mean-field theory.

The exchange pathways included in our Hamiltonian match those that would be obtained by projecting a Hubbard model to fourth order[37], except for the cyclic 4-spin terms that we have omitted for simplicity. In cuprates the 4-spin terms result in a zone boundary dispersion corresponding to an effective ferromagnetic J_2[38]; a similar effect may explain the ferromagnetic next-nearest intra-layer coupling J_2 reported in Sr_2IrO_4[8] and also found here in $Sr_3Ir_2O_7$. The strong inter-layer coupling $J_c = 90$ meV is qualitatively consistent with the very large bilayer splitting in the band structure measured by ARPES[39]. Concerning the ratio of inter- to intra-layer coupling $J_c/J = 3.5$, we note that in the SU(2) symmetric case, linear bond-operator theory overestimates the quantum critical ratio $J_c/J = 4$ [26] whereas numerical methods place it at 2.51[24]. It is therefore plausible that

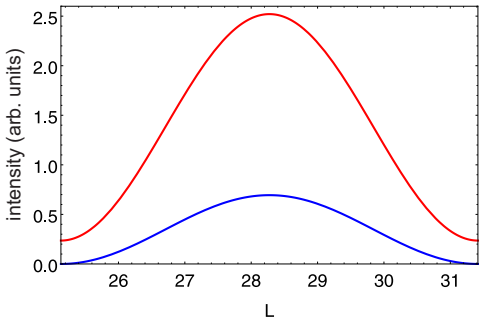

FIG. 6. Dependence of the longitudinal (blue) and transverse (red) intensities on the out-of-plane momentum L at the reciprocal space point (π, π).

treating our Hamiltonian to higher order would decrease the extracted ratio correspondingly by increasing J.

With this set of parameters, adjusted to fit the dispersion only, the intensities of the transverse and longitudinal modes (see Fig. 4(b)) are in reasonable agreement with the experimental results: the response peaks around (1/2,1/2), and the transverse mode is more intense across the whole Brillouin zone than the longitudinal one. However, our theory appears to overestimate the intensity of the transverse mode relative to the longitudinal one.

The L dependence of the RIXS spectrum has also been calculated (see Fig. 6) and is qualitatively in agreement with the data shown in Fig. 2(b). Indeed, the intensities vary periodically with q_c, reaching their maximum at $q_c = \pi$ ($L = 28.3$) (Fig.6). While I^T is finite for all momenta, I^L vanishes when q_c is a multiple of 2π. In particular, at $L = 25$, $q_c/2\pi = 6.1$, i.e. q_c is nearly a multiple of 2π, and the longitudinal intensity nearly vanishes, in agreement with the theoretical prediction. We believe that this explains why the D feature has not been detected in the previous experiment.

Finally, inserting the values for the coupling constants and the rotation angle $\chi = \frac{1}{2}\arccos\left(\frac{J_c}{4(J-J_2-J_3)}\right) \approx 25°$ into Eq.(12), we get a staggered magnetization of

$$\frac{g}{2}\,|\sin(2\chi)|\,|1-\alpha|\,\mu_B = 0.76\,\mu_B. \qquad (14)$$

In this formalism, the AF order is a consequence of the non-zero value of the rotation angle χ, which, in the groundstate, mixes singlets and triplets on a dimer. The correction due to quantum fluctuations is very small ($\alpha \approx 0.006$) because the spectrum has a large gap. As compared to the experimental value of about $0.52\pm0.08\mu_B$[40], the theoretical value is somewhat larger. It would be easy to get a smaller moment by choosing a smaller rotation angle χ at the expense of the quality of the fit of the dispersion. However, we have not attempted to do it since the bond-operator mean-field theory should not be considered as quantitatively accurate.

IV. CONCLUSION

Putting our results in perspective, we first recall that bilayer systems with SU(2)-symmetry have a quantum critical point (QCP) as a function of the interlayer coupling between an antiferromagnetic phase and a gapped phase (Fig. 1(d)). When anisotropy in spin space becomes important, as in systems with strong spin-orbit coupling such as $Sr_3Ir_2O_7$, a new paradigm arises where the quantum critical point is replaced by a simple transition between a gapped antiferromagnet and a gapped quantum dimer system, as sketched in Fig. 1(e). Considering the failure of linear spin-wave theory to explain the new mode reported in this paper together with the presence of a significant staggered magnetization, we are led to the conclusion that the system lies in the intermediate regime, on the left of the point where the antiferromagnetic order disappears, but with excitations of dominantly quantum dimer character. It will be rewarding to test this conclusion with more sophisticated theoretical approaches that could allow one to reach a fully quantitative agreement with experiments.

ACKNOWLEDGMENTS

We gratefully thank C. Henriquet and R. Verbeni for technical assistance during the experiements and B. Normand, O. Syljuaasen and B. Dalla Piazza for insightful discussions. The work in Lausanne was supported by the Swiss National Science Foundation and its Sinergia network Mott Physics Beyond the Heisenberg Model, in London by the EPSRC and in Würzburg by the ERC starters grant TOPOLECTRICS under ERC-StG-Thomale-336012.

[1] D. Pesin and L. Balents, Nat Phys **6**, 376 (2010).
[2] W. Witczak-Krempa, G. Chen, Y. B. Kim, and L. Balents, Annual Review of Condensed Matter Physics **5**, 57 (2014).
[3] B. Kim, H. Jin, S. Moon, J.-Y. Kim, B.-G. Park, C. Leem, J. Yu, T. Noh, C. Kim, S.-J. Oh, J.-H. Park, V. Durairaj, G. Cao, and E. Rotenberg, Phys. Rev. Lett. **101**, 076402 (2008).
[4] J. Kim, A. Said, D. Casa, M. Upton, T. Gog, M. Daghofer, G. Jackeli, J. van den Brink, G. Khaliullin, and B. Kim, Phys. Rev. Lett. **109**, 157402 (2012).
[5] J. Nichols, N. Bray-Ali, A. Ansary, G. Cao, and K.-W. Ng, Physical Review B **89**, 085125 (2014).
[6] B. J. Kim, H. Ohsumi, T. Komesu, S. Sakai, T. Morita, H. Takagi, and T. Arima, Science **323**, 1329 (2009).
[7] S. Boseggia, R. Springell, H. Walker, H. Rønnow, C. Rüegg, H. Okabe, M. Isobe, R. Perry, S. Collins, and D. McMorrow, Phys. Rev. Lett. **110**, 117207 (2013).
[8] J. Kim, D. Casa, M. Upton, T. Gog, Y.-J. Kim, J. Mitchell, M. van Veenendaal, M. Daghofer, J. van den Brink, G. Khaliullin, and B. Kim, Phys. Rev. Lett. **108**, 177003 (2012).
[9] M. Ge, T. F. Qi, O. B. Korneta, D. E. De Long, P. Schlottmann, W. P. Crummett, and G. Cao, Physical Review B **84**, 100402 (2011).
[10] J. G. Zhao, L. X. Yang, Y. Yu, F. Y. Li, R. C. Yu, Z. Fang, L. C. Chen, and C. Q. Jin, Journal of Applied Physics **103**, 103706 (2008).
[11] Y. Okada, D. Walkup, H. Lin, C. Dhital, T.-R. Chang, S. Khadka, W. Zhou, H.-T. Jeng, M. Paranjape, A. Bansil, Z. Wang, S. D. Wilson, and V. Madhavan, Nature materials **12**, 707 (2013).
[12] S. Boseggia, R. Springell, H. C. Walker, A. T. Boothroyd, D. Prabhakaran, D. Wermeille, L. Bouchenoire, S. P. Collins, and D. F. McMorrow, Phys. Rev. B **85**, 184432 (2012).
[13] J. W. Kim, Y. Choi, J. Kim, J. F. Mitchell, G. Jackeli, M. Daghofer, J. van den Brink, G. Khaliullin, and B. Kim, Phys. Rev. Lett. **109**, 037204 (2012).
[14] L. Ament, M. van Veenendaal, T. Devereaux, J. Hill, and J. van den Brink, Rev. Mod. Phys. **83**, 705 (2011).
[15] M. Moretti Sala, C. Henriquet, L. Simonelli, R. Verbeni, and G. Monaco, Journal of Electron Spectroscopy and Related Phenomena **188**, 150 (2
[16] X. Liu, V. M. Katukuri, L. Hozoi, W.-G. Yin, M. P. M. Dean, M. H. Upton, J. Kim, D. Casa, A. Said, T. Gog, T. F. Qi, G. Cao, A. M. Tsvelik, J. van den Brink, and J. P. Hill, Phys. Rev. Lett. **109**, 157401 (2012).
[17] M. Moretti Sala, S. Boseggia, D. F. McMorrow, and G. Monaco, Phys. Rev. Lett. **112**, 026403 (2014).
[18] M. Moretti Sala, K. Ohgushi, A. Al-Zein, Y. Hirata, G. Monaco, and M. Krisch, Phys. Rev. Lett. **112**, 176402 (2014).
[19] M. Moretti Sala, M. Rossi, A. Al-Zein, S. Boseggia, E. C. Hunter, R. S. Perry, D. Prabhakaran, A. T. Boothroyd, N. B. Brookes, D. F. McMorrow, G. Monaco, and M. Krisch, Phys. Rev. B **90**, 085126 (2014).
[20] H. Wang and J. Zhou, Journal of Applied Crystallography **38**, 830 (2005).
[21] K. Hida, Journal of the Physical Society of Japan **61**, 1013 (1992).
[22] A. J. Millis and H. Monien, Phys. Rev. Lett. **70**, 2810 (1993).
[23] A. J. Millis and H. Monien, Phys. Rev. B **50**, 16606 (1994).
[24] A. W. Sandvik and D. J. Scalapino, Phys. Rev. Lett. **72**, 2777 (1994).
[25] T. Miyazaki, I. Nakamura, and D. Yoshioka, Phys. Rev. B **53**, 12206 (1996).
[26] Sommer, T., Vojta, M., and Becker, K. W., Eur. Phys. J. B **23**, 329 (2001).
[27] C. J. Hamer, J. Oitmaa, and Z. Weihong, Phys. Rev. B **85**, 014432 (2012).
[28] S. Sachdev and R. Bhatt, Phys. Rev. B **41**, 9323 (1990).
[29] S. Gopalan, T. Rice, and M. Sigrist, Phys. Rev. B **49**, 8901 (1994).
[30] O. Sushkov and V. Kotov, Phys. Rev. Lett. **81**, 1941 (1998).

[31] P. Bouillot, C. Kollath, A. Läuchli, M. Zvonarev, B. Thielemann, C. Rüegg, E. Orignac, R. Citro, M. Klanjšek, C. Berthier, M. Horvatić, and T. Giamarchi, Phys. Rev. B **83**, 054407 (2011).
[32] G. Jackeli and G. Khaliullin, Phys. Rev. Lett. **102**, 017205 (2009).
[33] L. Shekhtman, O. Entin-Wohlman, and A. Aharony, Phys. Rev. Lett. **69**, 836 (1992).
[34] S. Boseggia, H. C. Walker, J. Vale, R. Springell, Z. Feng, R. S. Perry, M. M. Sala, H. M. Rønnow, S. P. Collins, and D. F. McMorrow, Journal of Physics: Condensed Matter **25**, 422202 (2013).
[35] D. G. Joshi, K. Coester, K. P. Schmidt, and M. Vojta, Phys. Rev. B **91**, 094404 (2015).
[36] D. G. Joshi and M. Vojta, Phys. Rev. B **91**, 094405 (2015).
[37] B. Dalla Piazza, M. Mourigal, M. Guarise, H. Berger, T. Schmitt, K. J. Zhou, M. Grioni, and H. M. Rønnow, Phys. Rev. B **85**, 100508 (2012).
[38] M. Guarise, B. Dalla Piazza, M. Moretti Sala, G. Ghiringhelli, L. Braicovich, H. Berger, J. Hancock, D. van der Marel, T. Schmitt, V. Strocov, L. Ament, J. van den Brink, P.-H. Lin, P. Xu, H. Rønnow, and M. Grioni, Phys. Rev. Lett. **105**, 157006 (2010).
[39] L. Moreschini, S. Moser, A. Ebrahimi, B. Dalla Piazza, K. S. Kim, S. Boseggia, D. F. McMorrow, H. M. Rønnow, J. Chang, D. Prabhakaran, A. T. Boothroyd, E. Rotenberg, A. Bostwick, and M. Grioni, Phys. Rev. B **89**, 201114 (2014).
[40] C. Dhital, S. Khadka, Z. Yamani, C. de la Cruz, T. Hogan, S. Disseler, M. Pokharel, K. Lukas, W. Tian, C. Opeil, Z. Wang, and S. Wilson, Phys. Rev. B **86**, 100401 (2012).